Article
Journal of Nanoscience and Nanotechnology
Vol. 21, 5653–5658, 2021
www.aspbs.com/jnn

Effect of Structural Deficiencies on Bi-Ferroic Behaviors of Lead-Free $Bi_{0.5}Na_{0.40}K_{0.10}TiO_3$ Films

Ngo Duc Quan[1,*], Nguyen Duc Minh[2,3], and Hoang Viet Hung[1,*]

[1] School of Engineering Physics, Hanoi University of Science and Technology, No. 1 Dai Co Viet, Hanoi 100000, Vietnam
[2] International Institute for Materials Science, Hanoi University of Science and Technology, No. 1 Dai Co Viet, Hanoi 100000, Vietnam
[3] MESA+ Institute for Nanotechnology, University of Twente, 7500AE Enschede, The Netherlands

Lead-free $Bi_{0.5}Na_{0.4}K_{0.1}TiO_3$ (BNKT) ferroelectric films on $Pt/Ti/SiO_2/Si$ substrates were prepared via a sol–gel spin coating routine. The microstructures and multiferroic behaviors of the films were examined intimately as a function of the annealing time. A rise of annealing time enhanced the crystallization of the films via the perovskite structure. The multiferroic behavior, including simultaneously the magnetic and ferroelectric orders, was observed altogether the films. When the annealing time rose, ferroelectric and magnetic properties were found significantly increased. The remnant polarization (P_r), also as maximum polarization (P_m) respectively increased to the very best values of 11.5 μC/cm^2 and 40.0 μC/cm^2 under an applied electric field of 500 kV/cm. The saturated magnetization (M_s) of films increased to 2.3 emu/cm^3 for the annealing time of 60 minutes. Oxygen vacancies, originating from the evaporation of metal ions during annealing at high temperatures are attributed to the explanation for ferromagnetism within the BNKT films.

Keywords: Multiferroic, Ferromagnetic, Ferroelectric, Lead-Free, BNKT.

1. INTRODUCTION

Multiferroic materials, new generation materials are being paid more attention because have potential for applications as magnetic field sensors, actuators, new types of electronic memory devices, and switches [1]. Multiferroic materials own unique property as magnetoelectricity (ME) stemmed from the existence of a coupling between electric dipolar and magnetic orders at room temperature [2]. Thanks to their special properties, multiferroics are studied largely for several technological applications, like magnetoelectric (ME) recording, magnetoelectric random access memories (MERAM), and electrically tunable microwave devices [3, 4]. By nature, it's found difficult to achieve simultaneously ferroelectricity and ferromagnetism in consequence of their opposite mechanisms [5]. Hence, by no means, the materials reveal the multiferroic behavior at room temperature. Many recent works have focused on lead-based materials $PbTiO_3$ (PTO) thanks to their outstanding properties, specially ferroelectricity. PTO materials doped the transition metals (as Fe, Mn or Ni, etc.) were reported to obtain the room-temperature ferromagnetism [6–9]. It's believed that the oxygen vacancies are liable for the room-temperature multiferroic behavior within the PTO materials [10]. Similar behavior was also detected in the composites [11] or heterolayer films [12] of PTO with the perovskite $CoFe_2O_4$. Nevertheless, PTO-based materials contain over 60 wt% Pb content that has likely put the environment, and human health in danger [13]. Therefore, the design of lead-free multiferroic materials with higher properties is highly required.

Recently, lead-free Bi-based ferroelectric materials, like $Bi_{0.5}Na_{0.5}TiO_3$ (BNT), $Bi_{0.5}K_{0.5}TiO_3$ (BKT), or $Bi_{0.5}(Na,K)_{0.5}TiO_3$ (BNKT) are widely studied because Bi^{3+} is very polarizable [14]. BNKT materials, within MPB (MPB is the morphotropic phase boundary) involving simultaneously rhombohedral ($R3c$) and tetragonal (P4 mm) phases [15–17] exhibited excellent electromechanical properties. Yuji et al. observed an outsized d_{33} (d_{33}, piezoelectric coefficient) of 167 pC/N, k_{33} (k_{33}, electromechanical coupling coefficient) of 0.56, and a high P_r value (P_r, remnant polarization) of 38 μC/cm^2 [18]. Especially, BNKT-based materials exposed the room temperature ferromagnetic behavior [19, 20]. With substituting Mn^{2+} for Ti^{4+}, Thanh et al. observed the room temperature ferromagnetism in BNT materials, which is stemmed

*Authors to whom correspondence should be addressed.

from oxygen vacancies [21]. BNT materials, substituted by Cr at the Ti-site revealed weak ferromagnetic behavior with the M_s value of 0.08 μB/Cr at room temperature [22]. Reported BNT samples in Ref. [23] revealed *M–H* curves without saturation when Fe-doped concentration is within the range of 1 mol% to 10 mol%. This result was contributed by the paramagnetic phase. Similarly, the pure $Bi_{0.5}K_{0.5}TiO_3$ materials, with the contribution of vacancies at *B* and/or O sites also show poor ferromagnetism at room temperature [24]. When doped by Fe, *M–H* curves of BKT transform from saturated shapes to unsaturated ones [25] because the paramagnetic phase is enhanced. Co-doped $Bi_{0.5}K_{0.5}TiO_3$ materials were reported in Ref. [26] disclosing the room-temperature ferromagnetism, with the saturation magnetization of 0.879 emu/g. It's also proved that BKT exhibits similar magnetic behavior when Ti^{4+}-site is substituted by other ions, like Mn^{2+} [20], Cr^{3+} [27]. The ferromagnetism in $Bi_{0.5}K_{0.5}TiO_3$ materials is stemmed from the presence of O or Ti vacancies or intrinsic defects.

Although BNKT materials revealed the multiferroic properties at room temperature, these behaviors are quite poor, and their origin was still unclear. Besides, processing factors, like annealing temperature, annealing time, film thickness are attributed to influence strong to physic properties of BNKT films [28–30]. During this work, the physical characteristics of $Bi_{0.5}Na_{0.4}K_{0.1}TiO_3$ (abbreviated as BNKT) films fabricated by employing a spin coating technique on $Pt/Ti/SiO_2/Si$ substrates were investigated as a function of annealing time (10, 20, 40, and 60 min). We found that the ferroelectric and magnetic behaviors of the films were significantly enhanced by increasing annealing time.

2. EXPERIMENTAL DETAILS

The $Bi_{0.5}Na_{0.4}K_{0.1}TiO_3$ (BNKT) films were deposited on $Pt/Ti/SiO_2/Si$ substrates by engaging a sol–gel technique. Here, the BNKT precursor solutions (concentration of 0.4 M) are prepared from raw materials as bismuth nitrate ($Bi(NO_3)_3 \cdot 5H_2O$, $\geq$98%, Sigma–Aldrich), potassium nitrate (KNO_3, $\geq$99%, Sigma–Aldrich), sodium nitrate ($NaNO_3$, $\geq$99%, Sigma–Aldrich), and titanium isopropoxide ($Ti[i\text{-}OPr]_4$, $\geq$99%, Sigma–Aldrich) with solvent including 2-methoxyethanol and acetylacetone. The BNKT films were formed by the subsequent steps: *i*/spin coating precursor on substrates at 4000 rpm was conducted for 30 second; *ii*/the films were pyrolyzed at 400 °C for 10 min; *iii*/the crystallization at 700 °C was occured for various times: 10 min, 20 min, 40 min, 60 min (named as S10, S20, S40, S60, respectively). The steps *i*/and *ii*/were repeatedly conducted until the films reaching the specified thickness.

After preparation, measurements were conducted to analyze physical characteristics of BNKT films. We employed a field emission scanning electron microscope (FE-SEM, Hitachi S4800) and atomic force microscopy (AFM, Bruker Dimension ICON) to examine surface morphologies of the films. The structural property of BNKT thin films was specified via a Bruker D5005 diffractometer with Cu-Kα cathode (λ = 1.5406 Å). Ferroelectric properties of the films were analyzed through *P–E* hysteresis loops measured by a TF Analyzer 2000 ferroelectric tester (aixACCT Systems GmbH, Germany) within the applied voltages range from −25 V to 25 V, frequency of 1000 Hz. The magnetic properties were detected with the Vibrating Sample Magnetometer (VSM, 7404, Lake Shore, USA).

3. RESULTS AND DISCUSSION

The surficial morphologies of the BNKT films were evaluated through AFM and FE-SEM images. Figure 1(a) shows 2D and 3D AFM images of BNKT films with annealing times, 10 min (S10), 20 min (S20), 40 min (S40), 60 min (S60). The physical parameters that describe the surface morphologies of BNKT films, like root mean square (*Rms*), surface skewness (*Ssk*), and coefficient of kurtosis (Ska) were achieved by the AFM analysis, shown in Table I. Where *Rms* is a physical parameter illustrating the surface roughness level of the films. *Ssk*, a statistical parameter characterizes the extent of symmetry of the surface heights. The kurtosis coefficient, *Ska* is a statistical measure to match a random distribution of peak heights and pore depths. AFM images showed that BNKT films possess relatively smooth and continuous surfaces. The evidence is all the films exhibit small *Rms* values from 3.78 nm to 5.58 nm (Table I). For the films annealed for 10 min, the amount of peaks prevails that of pores, confirmed by surface skewness factor, $Ssk > 0$ [31]. The amount of peaks declines when the annealing time increases. This observation is according to the decreasing trend of *Ssk* to approximately zero. *Ska* values range from 2.20 to ~3 proving that BNKT films haven't any presence of anomaly high peaks/deep valleys. Figure 1(b) demonstrates surficial and cross-sectional SEM images of film annealed for 60 min. S60 film reveals a dense microstructure and no traces of cracks were detected. Grains are uniformly distributed on the whole surface with grain boundaries being obvious defined. Film thicknesses, evaluated by cross-sectional FE-SEM images are around 300 nm.

XRD patterns for BNKT films are demonstrated in Figure 2(a) with the 2θ ranges of 28°–72°. All the samples show sharp diffraction peaks characterizing for the perovskite structure, like (110), (200), (211) and (300). The (111) peak, exhibiting the highest intensity, fits to the Pt-coated substrate. No traces of impurity phases are observed. This result agrees with the previous reports, that exposed that the BNKT films possess the MPB composition at Na/K rate of 80/20 [13–14, 28]. A magnification of X-ray diffraction patterns at 2θ of around 31°, 40° and 47° focuses on the (200) preferred orientations to analyze intimately the influence of the annealing time on film

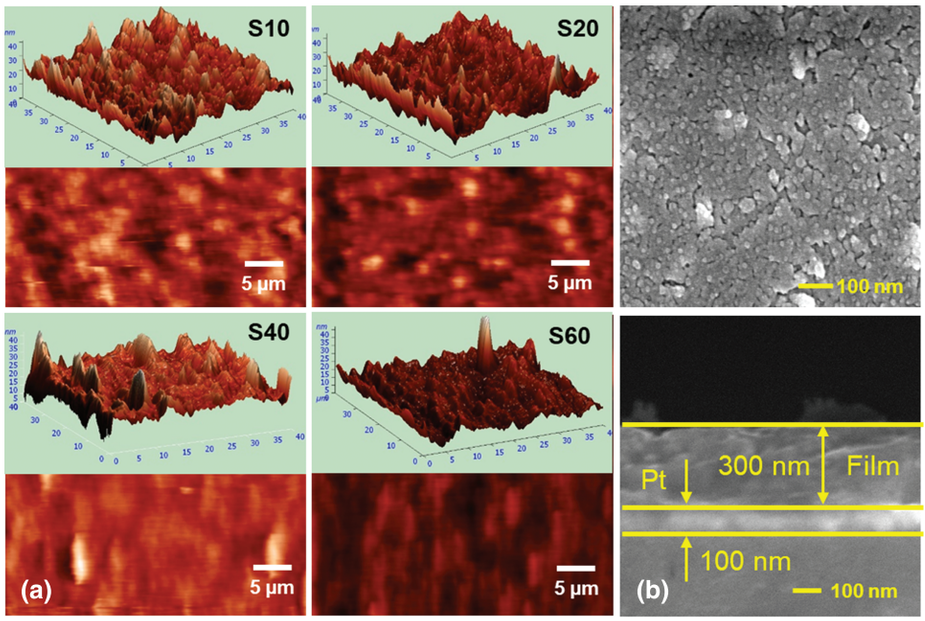

Figure 1. (a) 2D–3D AFM images of BNKT films annealed at different times: S10, S20, S40, S60; (b) FE-SEM micrographs of sample S60 and Cross-sectional SEM image of sample S60.

structures (Fig. 2(a)). For sample S10, the intensity of the (200) peak is low. This is often caused by structural disorder because annealing time isn't long enough for crystallization to occur completely. As a result, BNKT film may possess the intermediate phase [32]. It was observed from the figure that the (200) peak became sharper and its intensity was continuously increased when the annealing time was raised. This indicated that crystallization in films was enhanced with rise of annealing time.

The polarization hysteresis (P–E) loops of the BNKT films with annealing times: 10, 20, 40, 60 min are shown in Figure 3(a). The maximal polarization (P_m), remnant polarization (P_r), and coercive electric field (E_c) are plotted as a function of annealing time in Figure 3(b). With well-shaped P–E hysteresis loops, all the film samples exhibit a typical ferroelectric behavior at room temperature. The E_c value shows a little change with a rise of the annealing time. It fluctuates between 77.0 kV/cm to 84.8 kV/cm when the annealing time increases from 10 min to 60 min. However, the P_m, and P_r values significantly increase with increasing the annealing time. For the sample S10, P_r and P_m values are relatively poor around 5.5 μC/cm^2 and 24.8 μC/cm^2, respectively. P_r and P_m are significantly enhanced and reach their highest values of 11.5 μC/cm^2 and 40.0 μC/cm^2, respectively with the annealing time of 60 min. So, the ferroelectricity of BNKT films has been considerably enhanced by a rise of the annealing time. This improvement is mainly thanks to the annealing time is long enough for the crystallization to occur completely.

Figures 4(a)–(d) plots the magnetic hysteresis (M–H) loops of BNKT films corresponding the annealing times. All the sample were measured at the same magnetic field of 5 kOe in the room-temperature. Observation of M–H loops at room-temperature indicated that magnetic order exists in BNKT films. Film S10 exhibits poor ferromagnetic behavior with its saturated magnetization (M_s) value of 1.4 emu/cm^3. This is often contributed by the competition between antiferromagnetic and paramagnetic orders. Hung et al. observed this paramagnetic behavior in BNT materials [33] and reported that the $3d^\circ$ empty state of

Table I. The physical parameters morphologically typify the samples.

Samples	S10	S20	S40	S60
Root mean square, *Rms*	5.58	4.86	4.65	3.87
Surface skewness, *Ssk*	0.29	0.11	0.09	0.03
Coefficient of kurtosis, *Ska*	2.20	2.34	3.16	3.01
P_r (μC/cm^2)	5.5	6.0	8.7	11.5
P_m (μC/cm^2)	24.8	27.6	36.4	40.0

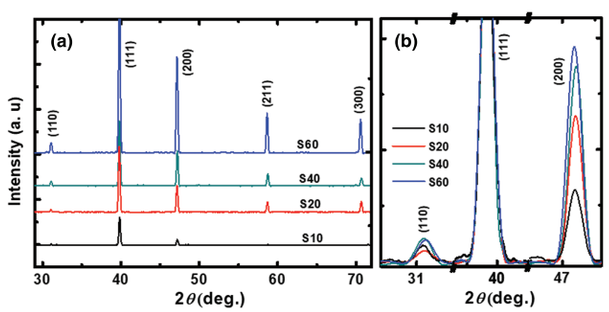

Figure 2. (a) X-ray diffraction patterns of BNKT films in the 2θ ranges of 28°–72° and (b) around 31°, 41°, 47°.

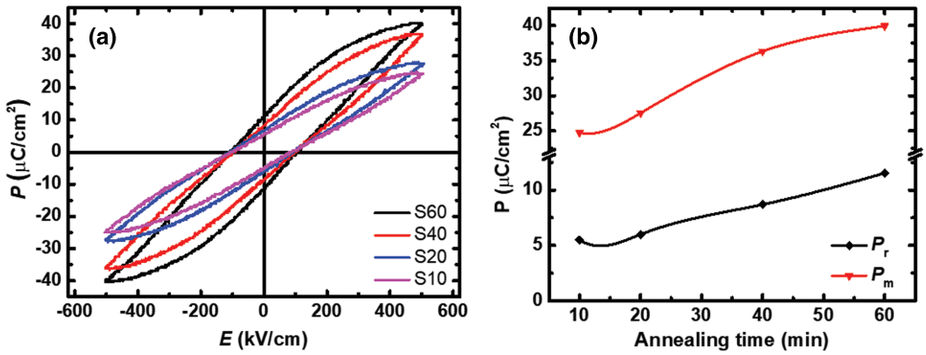

Figure 3. (a) *P–E* ferroelectric hysteresis loops of BNKT films at the same applied electric field of 500 kV/cm, (b) the maximum polarization (P_m) and remnant polarization (P_r) of BNKT films.

Ti^{4+} is liable for paramagnetic property [34]. Additionally, previous studies indicated that Ti^{4+} and Ti^{3+} cations coexist within the crystal lattice BNKT [35–38]. It's supposed that the direct exchange coupling Ti^{3+}–O–Ti^{3+} contributes to the antiferromagnetic order [39]. However, M_s value was significantly enhanced when annealing temperature was risen. It reached to the best value of 2.3 emu/cm^3 for film S60. The magnetic dipole moments originated by the oxygen deficiencies were attributed to contribute to the improvement of the ferromagnetic behavior within the BNKT films [2, 40]. Theoretically, Stoneham et al. [41] proved that magnetic orders also are related to point deficiencies like cation or anion vacancies. The origin of point defects in BNKT crystal is contributed by the loss of metal ions at *A*-site like Bi^{3+}, Na^+, or K^+ as annealed at high temperature. Chemically, the Bi and Na loss are often described as follows:

$$Bi_{loss} \rightarrow 2V'''_{Bi} + 3V^{\bullet\bullet}_{O} \quad (1)$$

$$Na/K_{loss} \rightarrow 2V'_{Na/K} + V^{\bullet\bullet}_{O} \quad (2)$$

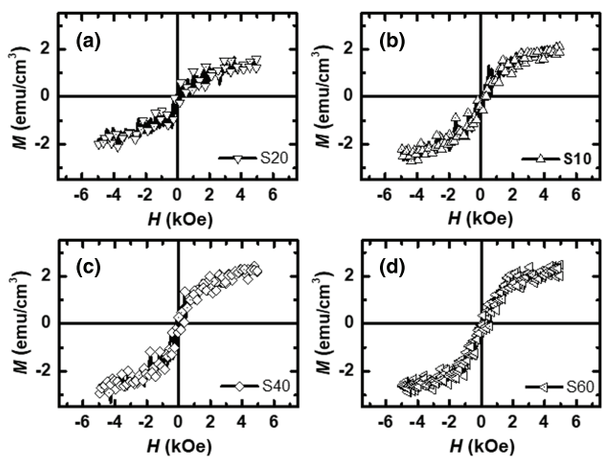

Figure 4. Room-temperature magnetic hysteresis (M–H) loops of BNKT films annealed with the different durations: (a) 10 min, (b) 20 min, (c) 40 min, and (d) 60 min at the applied magnetic field of 5 kOe.

Where, V'''_{Bi}, V'_{Na} and V'_{K} là are point defects corresponding to Bi, Na and K loss; $V^{\bullet\bullet}_{O}$ is oxygen vacancy. The point defects formed the super-exchange interaction of Ti^{3+} through oxygen vacancies (Ti^{3+}–$V^{\bullet\bullet}_{O}$–Ti^{3+}). Coey et al. testified that the effective radius of hybrid orbital influences strongly the interaction of magnetic ions through oxygen vacancies [42]. Hence, the ferromagnetic interaction within the BNKT films was improved thanks to Ti^{3+} cations controlled the interaction and distance of magnetic ions through oxygen vacancies. Figure 5 presents a diagram representation of the impact of the oxygen vacancy $V^{\bullet\bullet}_{O}$ on the experimental magnetic ordering observed for BNKT films. The right part illustrates the electron interaction via oxygen atomic and vacancy states verifying the spin-orientation described in the left one. Weiss et al. supposed that the blending between transition metal 3*d* and oxygen 2*p* orbitals that permits virtual electron transfer between magnetic centers, causes the *B*–O-*B* (where *B* is Ti^{3+} and/or Ti^{4+}) antiferromagnetic exchange coupling [43]. This direct exchange coupling is liable for

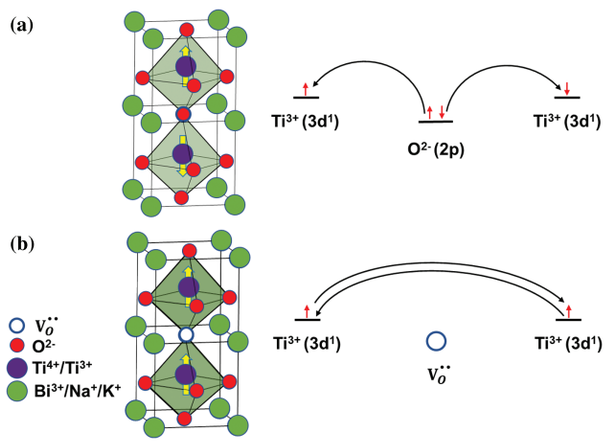

Figure 5. A schematic representation revealing the nature of antiferromagnetic and ferromagnetic orders in (a) original and (b) defective BNKT material. The right part illustrates the electron interaction mediated by oxygen atomic and vacancy states affirming the magnetic spin moment illustrated in the left one.

the reverse spin arrangement neighboring the oxygen and causing antiferromagnetic behaviors. However, when oxygen vacancies occurred, the charge carriers involved in bonding mediate the super-exchange interaction between the local spins via oxygen vacancies (Ti^{3+}–$V_O^{\bullet\bullet}$–Ti^{3+}). The super-exchange interaction makes possible the magnetic moment neighboring oxygen vacancies to align in the parallel direction and forming ferromagnetic orders.

4. CONCLUSIONS

Multiferroic $Bi_{0.5}Na_{0.4}K_{0.1}TiO_3$ (BNKT) films were successfully synthesized on Pt–Si substrates via spin-coating technique. BNKT films were well crystallized with the perovskite structure when annealing time rises. It was observed that BNKT films show multiferroic behavior at room temperature. A rise of annealing time to 60 minutes enhanced the ferroelectric and magnetic properties of the films. Under an applied electric field of 500 kV/cm, the ferroelectric parameters as P_m and P_r were enhanced to their highest values of 40.0 μC/cm^2 and 11.5 μC/cm^2, respectively. This improvement is mainly thanks to the crystallization in films was occurred completely. BNKT-films annealed for 60 minutes shows the best ferromagnetic characteristic with the saturated magnetization (M_s) of 2.3 emu/cm^3. Point defects as cation or anion vacancies promoted by the loss of metal ions at *A*-site are the derivation of ferromagnetic behaviors in BNKT. Room temperature ferromagnetism makes these BNKT films possess more potential in multiferroic and spintronic applications.

Conflicts of Interest

The authors declare no conflicts of interest.

Acknowledgments: This research is funded by the Nippon Sheet Glass Foundation and Hanoi University of Science and Technology (HUST) under project number T2020-PC-057.

References and Notes

1. Ramesh, R. and Spaldin, N.A., **2007**. Multiferroics: Progress and prospects in thin films. *Nature Materials*, *6*(1), pp.21–29.
2. Quan, N.D., Toan, T.Q., Hung, V.N. and Nguyen, M.-D., **2019**. Influence of crystallization temperature on structural, ferroelectric and ferromagnetic properties of lead-free $Bi_{0.5}(Na_{0.8}K_{0.2})_{0.5}TiO_3$ multiferroic films. *Advances in Materials Science and Engineering*, *2019*, pp.1–10.
3. Eerenstein, W., Mathur, N.D. and Scott, J.F., **2006**. Multiferroic and magnetoelectric materials. *Nature*, *442*(7104), pp.759–765.
4. Lu, C., Hu, W., Tian, Y. and Wu, T., **2015**. Multiferroic oxide thin films and heterostructures. *Applied Physics Reviews*, *2*(2), p.021304.
5. Spaldin, N.A. and Fiebig, M., **2005**. Materials science. The renaissance of magnetoelectric multiferroics. *Science*, *309*(5733), pp.391–392.
6. Ren, Z., Xu, G., Wei, X., Liu, Y., Hou, X., Du, P., Weng, W., Shen, G. and Han, G., **2007**. Room-temperature ferromagnetism in Fe-doped $PbTiO_3$ nanocrystals. *Applied Physics Letters*, *91*(6), p.063106.
7. Verma, K.C., Kotnala, R.K. and Negi, N.S., **2008**. Improved dielectric and ferromagnetic properties in Fe-doped $PbTiO_3$ nanoparticles at room temperature. *Applied Physics Letters*, *92*(15), p.152902.
8. Oanh, L.M., Do, D.B., Phu, N.D., Mai, N.T.P. and Minh, N.V., **2014**. Influence of Mn doping on the structure, optical, and magnetic properties of $PbTiO_3$ material. *IEEE Transactions on Magnetics*, *50*(6), pp.1–4.
9. Zhou, W., Deng, H., Yu, L., Yang, P. and Chu, J., **2015**. Magnetism switching and band-gap narrowing in Ni-doped $PbTiO_3$ thin films. *Journal of Applied Physics*, *117*, p.194102.
10. Shimada, T., Uratani, Y. and Kitamura, T., **2012**. Vacancy-driven ferromagnetism in ferroelectric $PbTiO_3$. *Applied Physics Letters*, *100*(16), p.162901.
11. Wang, B.Y., Wang, H.T., Singh, S.B., Shao, Y.C., Wang, Y.F., Chuang, C.H., Yeh, P.H., Chiou, J.W., Pao, C.W., Tsai, H.M., Lin, H.J., Lee, J.F., Tsai, C.Y., Hsieh, W.F., Tsai, M.H. and Pong, W.F., **2013**. Effect of geometry on the magnetic properties of $CoFe_2O_4$–$PbTiO_3$ multiferroic composites. *RSC Advances*, *3*(21), pp.7884–7893.
12. Murakami, M., Chang, K.S., Aronova, M.A., Lin, C.L., Yu, M.H., Simpers, J.H., Wuttig, M., Takeuchi, I., Gao, C., Hu, B., Lofland, S.E., Knauss, L.A. and Bendersky, L.A., **2005**. Tunable multiferroic properties in nanocomposite $PbTiO_3$–$CoFe_2O_4$ epitaxial thin films. *Applied Physics Letters*, *87*(11), p.112901.
13. Quan, N.D., Hung, V.N., Kim, I.W. and Dung, D.D., **2016**. Bipolar electric field induced strain in Li substituted lead-free $Bi_{0.5}(Na_{0.82}K_{0.18})_{0.5}Ti_{0.95}Sn_{0.05}O_3$ piezoelectric ceramics. *Journal of Nanoscience and Nanotechnology*, *16*(8), pp.7978–7982.
14. Quan, N.D., Hung, V.N. and Dung, D.D., **2017**. Effect of Zr doping on structural and ferroelectric properties of lead-free $Bi_{0.5}(Na_{0.80}K_{0.20})_{0.5}TiO_3$ films. *Journal of Electronic Materials*, *46*(10), pp.5814–5819.
15. Eitel, R.E., Clive, A.R., Thomas, R.S., Paul, W., Wes, H. and Seung-Eek, P., **2001**. New high temperature morphotropic phase boundary piezoelectrics based on Bi(Me)O_3–$PbTiO_3$ ceramics. *Japanese Journal of Applied Physics*, *40*(10R), pp.5999–6002.
16. Quan, N.D., Huu Bac, L., Thiet, D.V., Hung, V.N. and Dung, D.D., **2014**. Current development in lead-free Bi0.5(Na, K)0.5TiO_3-based piezoelectric materials. *Advances in Materials Science and Engineering, 2014*, pp.1–13.
17. Quan, N.D., Hong, N.V., Toan, T.Q. and Hung, V.N., **2018**. Enhanced ferroelectric properties and energy storage density in PLZT/BNKT heterolayered thin films prepared by sol–gel method. *European Physical Journal B*, *91*, p.316.
18. Yuji, H., Tomomi, W., Hajime, N. and Tadashi, T., **2008**. Piezoelectric properties of $(Bi_{1/2}Na_{1/2})TiO_3$-based solid solution for lead-free high-power applications. *Japanese Journal of Applied Physics*, *47*(9S), pp.7659–7663.
19. Wang, Y., Xu, G., Yang, L., Ren, Z., Wei, X. and Weng, W., **2009**. *Materials Science*, *27*, pp.471–476.
20. Tuan, N.H., Thiet, D.V., Odkhuu, D., Bac, L.H., Binh, P.V. and Dung, D.D., **2017**. Defect induced room temperature ferromagnetism in lead-free ferroelectric $Bi_{0.5}K_{0.5}TiO_3$ materials. *Physica B: Condensed Matter*, *532*, pp.108–114.
21. Thanh, L.T.H., Doan, N.B., Bac, L.H., Thiet, D.V., Cho, S., Bao, P.Q. and Dung, D.D., **2017**. Making room-temperature ferromagnetism in lead-free ferroelectric $Bi_{0.5}Na_{0.5}TiO_3$ material. *Materials Letters*, *186*, pp.239–242.
22. Thanh, L.T.H., Doan, N.B., Dung, N.Q., Cuong, L.V., Bac, L.H., Duc, N.A., Bao, P.Q. and Dung, D.D., **2017**. Origin of room temperature ferromagnetism in Cr-doped lead-free ferroelectric $Bi_{0.5}Na_{0.5}TiO_3$ materials. *Journal of Electronic Materials*, *46*(6), pp.3367–3372.
23. Wang, Y., Xu, G., Ji, X., Ren, Z., Weng, W., Du, P., Shen, G. and Han, G., **2009**. Room-temperature ferromagnetism of Co-doped $Na_{0.5}Bi_{0.5}TiO_3$: Diluted magnetic ferroelectrics. *Journal of Alloys and Compounds*, *475*(1), pp.L25–L30.

24. Li, Y., Moon, K.-S. and Wong, C.P., **2005**. Electronics without lead. *Science*, *308*(5727), pp.1419–1420.

25. Dung, D.D., Thiet, D.V., Odkhuu, D., Cuong, L.V., Tuan, N.H. and Cho, S., **2015**. Room-temperature ferromagnetism in Fe-doped wide band gap ferroelectric $Bi_{0.5}K_{0.5}TiO_3$ nanocrystals. *Materials Letters*, *156*, pp.129–133.

26. Cuong, L.V., Tuan, N.H., Odkhuu, D., Van Thiet, D., Dung, N.H., Bac, L.H. and Dung, D.D., **2017**. Observation of room-temperature ferromagnetism in Co-doped $Bi_{0.5}K_{0.5}TiO_3$ materials. *Applied Physics A*, *123*(8), p.563.

27. Tuan, N.H., Anh, V.K., Doan, N.B., Bac, L.H., Dung, D.D. and Odkhuu, D., **2018**. Theoretical and experimental studies on the influence of Cr incorporation on the structural, optical, and magnetic properties of $Bi_{0.5}K_{0.5}TiO_3$ materials. *Journal of Sol–Gel Science and Technology*, *87*(3), pp.528–536.

28. Quan, N.D., Hung, V.N. and Dung, D.D., **2017**. Influence of film thickness on ferroelectric properties and leakage current density in lead-free $Bi_{0.5}(Na_{0.80}K_{0.20})_{0.5}TiO_3$ films. *Materials Research Express*, *4*(8), p.086401.

29. Co, N.D., Cuong, L.V., Tu, B.D., Thang, P.D., Dien, L.X., Hung, V.N. and Quan, N.D., **2019**. Effect of crystallization temperature on energy-storage density and efficiency of lead-free $Bi_{0.5}(Na_{0.8}K_{0.2})_{0.5}TiO_3$ thin films prepared by Sol-gel method. *Journal of Science: Advanced Materials and Devices*, *4*(3), pp.370–375.

30. Quan, N.D., Toan, T.Q. and Hung, V.N., **2019**. Influence of crystallization time on energy-storage density and efficiency of lead-free $Bi_{0.5}(Na_{0.8}K_{0.2})_{0.5}TiO_3$ thin films. *Advances in Condensed Matter Physics*, *2019*, pp.1–8.

31. Nechifor, C.-D., Dorohoi, D.-O. and Ciobanu, C., **2009**. The influence of gamma radiations on physico-chemical properties of some polymer membranes. *Romanian Journal of Physics*, *54*, pp.349–359.

32. Chen, P., Wu, S., Li, P., Zhai, J. and Shen, B., **2018**. The phase formaTiOn process of $Bi_{0.5}(Na_{0.8}K_{0.2})_{0.5}TiO_3$ thin films prepared using the sol–gel method. *Ceramics International*, *44*(6), pp.6402–6408.

33. Hung, N.T., Bac, L.H., Trung, N.N., Hoang, N.T., Van Vinh, P. and Dung, D.D., **2018**. Room-temperature ferromagnetism in Fe-based perovskite solid solution in lead-free ferroelectric $Bi_{0.5}Na_{0.5}TiO_3$ materials. *Journal of Magnetism and Magnetic Materials*, *451*, pp.183–186.

34. Thanh, L.T.H., Doan, N.B., Bac, L.H., Thiet, D.V., Cho, S., Bao, P.Q. and Dung, D.D., **2017**. Making room-temperature ferromagnetism in lead-free ferroelectric $Bi_{0.5}Na_{0.5}TiO_3$ material. *Materials Letters*, *186*, pp.239–242.

35. Liu, X., Fan, H., Shi, J. and Li, Q., **2015**. Origin of anomalous giant dielectric performance in novel perovskite: $Bi_{(0.5-x)}La_xNa_{(0.5-x)}Li_xTi_{(1-y)}MyO_3$ ($M = Mg^{2+}$, Ga^{3+}). *Scientific Reports*, *5*, p.12699.

36. Shao, D.F., Yang, J., Zhu, X.B., Dai, J.M., Yang, Z.R., Song, W.H. and Sun, Y.P., **2012**. Observation of spin glass behavior in $Ba_{0.8}La_{0.2}Ti_{0.8}Co_{0.2}O_3$. *European Physical Journal B*, *85*(5), p.156.

37. Awan, M.Q., Ahmad, J., Berlie, A. and Liu, Y., **2018**. Influence of oxidation number of manganese on magnetic properties of lead free piezoelectric BNT ceramics. *Digest Journal of Nanomaterials and Biostructures*, *13*(1), pp.67–75.

38. Raengthon, N., Rujijanagul, G. and Cann, D.P., **2018**. Influence of a-site deficiency on electrical characteristics of barium strontium titanate perovskite dielectrics. *Journal of Applied Physics*, *124*(15), p.154105.

39. Quan, N.D., Minh, N.D. and Rijnders, G., **2020**. Influence of $BiFeO_3$ perovskite on the structure and magnetic properties of lead-free $Bi_{0.5}Na_{0.4}K_{0.1}TiO_3$ films. *Japanese Journal of Applied Physics*, *60*(1), p.010902.

40. Sundaresan, A., Bhargavi, R., Rangarajan, N., Siddesh, U. and Rao, C.N.R., **2006**. Ferromagnetism as a universal feature of nanoparticles of the otherwise nonmagnetic oxides. *Physical Review B*, *74*(16), p.161306.

41. Stoneham, A.M., Gavartin, J., Shluger, A.L., Kimmel, A.V., Ramo, D.M., Rønnow, H.M., Aeppli, G. and Renner, C., **2007**. Trapping, self-trapping and the polaron family. *Journal of Physics: Condensed Matter*, *19*(25), p.255208.

42. Coey, J.M.D., Venkatesan, M. and Fitzgerals, C.B., **2005**. Donor impurity band exchange in dilute ferromagnetic oxides. *Nature Materials*, *4*, pp.173–179.

43. Weiss, A., **1964**. Magnetism and the chemical bond. *Berichte der Bunsen-Gesellschaft für Physikalische Chemie*, *68*(10), pp.996–996.

Received: 27 March 2021. Accepted: 6 April 2021.